Predictive battery thermal management using quantile convolutional neural networks

Andreas M. Billert [*,a,b], Stefan Erschen [b], Michael Frey [a], Frank Gauterin [a]

[a] *Karlsruhe Institute of Technology (KIT), Institute of Vehicle System Technology, 76131 Karlsruhe, Germany*
[b] *Bayerische Motoren Werke AG, 80788 Munich, Germany*

ARTICLE INFO

ABSTRACT

An improvement in energy efficiency of Battery Thermal Management Systems (BTMS) can increase range and reduce well-to-wheel emissions of Battery Electric Vehicles (BEV). In this work, the potential of a predictive BTMS using Quantile Convolutional Neural Networks (QCNN) was examined. The QCNN provided quantile predictions of battery temperature based on input data from both previous and following drive segments. The predictive control was designed to choose battery cooling thresholds based on a weighted sum of battery cooling, ageing and derating costs derived by the quantile predictions. The predictive BTMS was analyzed concerning its adaptability to different routes ahead, tunability of cost weights as well as robustness to uncertainty of inputs. A setup with unchanged ageing costs reduced average cooling costs by 9% compared to a fixed threshold strategy in a set of 18 scenarios. Simplifications and limitations were discussed to provide a base for further improvements, for example concerning the limited freedom of cooling threshold choice. In conclusion, the developed framework was able to use QCNN predictions to increase the BTMS energy efficiency while taking ageing and derating effects into account.

1. Introduction

Driven by emission reduction goals, the share of Battery Electric Vehicles (BEV) is steadily rising and expected to surpass the worldwide share of passenger cars with combustion engine by 2040 [1]. Improving the energy efficiency of BEV can further reduce well-to-wheel emissions and provide higher ranges [2]. This motivates to develop more efficient Battery Thermal Management Systems (BTMS) considering their impact on energy consumption [3].

A predictive BTMS can reduce the energy consumption compared to an on-off controller with fixed hysteresis thresholds [4,5]. If the prediction shows a relatively low increase in battery temperature, active battery cooling and the corresponding energy consumption may be avoided. It can be based on physical or stochastic models [5–9]. Stochastic model predictive control incorporates statistical information about the prediction horizon, such as chance constraints or empirical probability distributions (e.g. of battery heat generation) [4,10]. Chance constraints assume time-independent distribution functions and scenario-based methods focus on the expectation value, which are both strong simplifications [10].

Predictive control with large prediction horizons is favorable concerning the search for a global optimum and provides enough time for the BTMS to anticipate upcoming events [11]. On the other hand, large horizons can be computationally expensive for classic model predictive control. This can be addressed by a two-layer control, for example combining model predictive control with dynamic programming as in [12] or with other global planning methods [11].

Predictive control based on Neural Networks (NN) shows further potential due to their aptitude to represent complex, nonlinear systems such as BTMS [13–15]. An improved performance of predictive control using NN is also observed for vehicle power control and vehicle dynamics [16–19], as well as for thermal management of buildings [20] and for heat exchangers [21]. This motivates the usage of a Quantile Convolutional Neural Network (QCNN) for battery temperature prediction in a predictive BTMS control, as described in [22]. The QCNN provides quantile predictions for five different battery cooling thresholds over a prediction horizon of 20 km in a sample size of 250 m. Thus, the cooling thresholds can be utilized as control parameter in a predictive control. The prediction uncertainty can be directly included, without the assumption of fixed distribution functions or expectation values.

* Corresponding author.
E-mail addresses: andreas.billert@partner.kit.edu (A.M. Billert), stefan.erschen@bmw.de (S. Erschen), michael.frey@kit.edu (M. Frey), frank.gauterin@kit.edu (F. Gauterin).

Nomenclature

Latin Symbols

A	Surface
c	Heat capacity; costs
h	Heat transfer coefficient
k	Horizon size
m	Mass
$\dot{Q}$	Heat transfer rate
R	Inner resistance
s	Drive distance
T	Temperature
t	Time
w	Weight

Greek Symbols

δ	Partial derivative
μ	Mean value
σ	Standard deviation
τ	Constant in cooldown function
θ	Slope angle

Subscripts

a	Ageing
amb	Ambient
b	Battery
c	Control; cooling
cool,e	Threshold to end cooling
cool,s	Threshold to start cooling
cooldown	Cool down

d	Derating
end	End
eod	End of drive
i	Index i, related to horizon step
init	Initial value
p	Specific value (of heat capacity)
q	Quantile
s	Surrounding
t	Total

Abbreviations and Acronyms

BEV	Battery Electric Vehicle
BTMS	Battery Thermal Management System
D	Dynamic profile, refers to US06
DOE	Design Of Experiments
eod	End of drive
FMU	Functional Mock-up Unit
H	Highway part of Artemis profile
LD	Less Dynamic
MD	More Dynamic
MSE	Mean Squared Error
NN	Neural Network
QCNN	Quantile Convolutional Neural Network
R	Rural part of Artemis profile
RAM	Random Access Memory
SOC	State Of Charge
SOH	State Of Health
T	Tsirakis profile
U	Urban part of Artemis profile

Model predictive control (for BTMS) can choose control parameters (e.g. battery cooling activation) in order to minimize predefined cost functions within a moving horizon [8,9]. Such cost functions can represent cooling energy consumption or temperature-related increase in ageing. Cost weights determine the balance between the contradicting goals of reducing energy consumption and keeping the battery temperature in a range of low ageing. Cooling costs can be derived from the energy consumption of BTMS components. Ageing costs can be calculated based on empirical relations as given by [23] and [24] and as done in [8,9,14]. They can incorporate the effect that high battery temperatures accelerate cyclic and calendric ageing. Temperature-dependent limitation of maximum available battery power, also called derating, can significantly reduce battery ageing [25,26]. On the other hand, the limitation of charge or discharge current results in reduced vehicle dynamics and charging performance, which can be addressed by including derating costs.

An analysis of a predictive BTMS can consider its adaptability to different drive profiles, tunability of its design parameters as well as robustness to inaccurate predictions of the system behavior [5,6,27]. Adaptability to different speed and height profiles is expected, considering their impact on energy consumption, and hence battery temperature [8,28]. The effect of varied design parameters (e.g. cost weights or set points) on contradicting cost goals or cost-related quantities can be visualized using Pareto curves in order to find the most suitable parameters [5,29]. Robustness analysis deals with the impact of inaccurate or noisy predictions on controller performance [27]. For instance, a Gaussian noise can be added on the foresight speed data which is used as predictive control input [11].

In this work, a predictive BTMS is presented, which uses the best performing QCNN from [22] for battery temperature prediction. It considers costs for cooling energy consumption, ageing and power derating to choose the most suitable battery cooling threshold at each

control interval. In contrast to classic model predictive control, the prediction uncertainty is directly given by the prediction model and can be included in the calculation of costs. The limited choice of control values in form of hysteresis thresholds reduces complexity in the optimization process and allows larger control intervals and prediction horizons. Therefore, the focus of this work is a more strategic view on predictive BTMS with a large horizon. The predictive control is tested and analyzed for various drive profiles concerning its adaptability, tunability and robustness. Discussion and conclusion provide a further outlook on current potentials and limitations and build the base for an optimization in a future work.

2. Method

In this chapter, a framework of a predictive BTMS is described. Fig. 1 depicts the elements of the framework. The vehicle is represented by a black-box simulation model as Functional Mock-up Unit (FMU). At each iteration, its outputs are processed for further usage in the loop and as output to enable further analysis after the simulation. The given drive profile leads to an update of parameters. Each time when a defined control distance s_c is passed, a QCNN predicts the battery temperature for different battery cooling thresholds as quantiles over a fixed prediction horizon. The total costs over the prediction horizon are calculated based on the predicted quantiles for each threshold. The battery cooling threshold with lowest total costs is chosen as new threshold and updated in the vehicle model. The simulation ends when the total distance of the given profile s_{end} is reached. Each step is further explained in the following paragraphs.

2.1. Data processing

In each iteration, simulation output from the vehicle model is
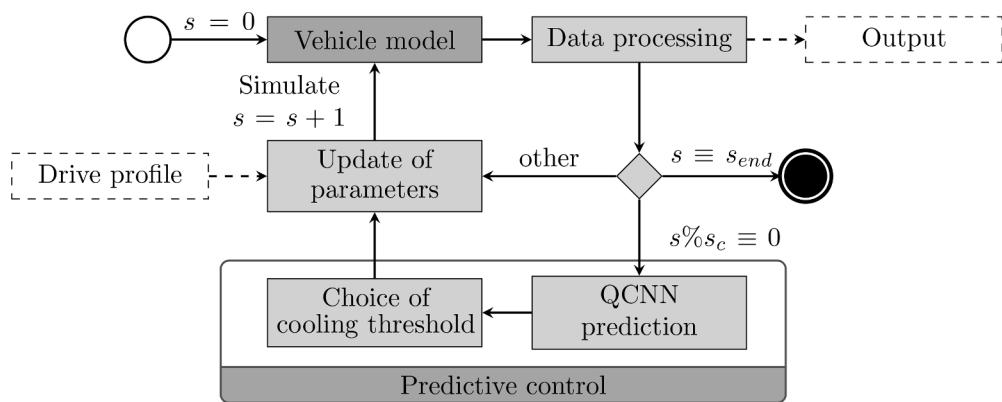
Fig. 1. Control framework including a vehicle model and a QCNN for battery temperature prediction. A predictive control is conducted each time when the driven distance s passed the control distance s_c and when the total distance s_{end} of the profile is not reached yet.

sampled into 250 m segments. At the beginning of the drive or when the control distance s_c is reached, all input data for the QCNN need to be prepared, also sampled to 250 m segments. This includes the data from previous segments as history data and the remaining drive profile as foresight input data. Engineered features are added to complete the set of input features. All input data are shaped into a history horizon size of 5 km and to a foresight horizon size of 20 km. If all previous segments do not cover 5 km or if the remaining drive is less than 20 km, the missing values are set to zero and masked in the horizon input feature. For the first prediction at time 0, the history input data of ambient and battery temperature are set to their initial values. All data are normalized by the same normalization factors that were used for training and testing the QCNN.

The control distance s_c is derived from the QCNN test metrics per horizon size, which are shown in Fig. 2. The quantile related metrics depict the occurrence of true values within and outside of the predicted quantiles and quantile intervals. Both quantile related metrics show bad performance for very small horizon sizes with few change in battery temperature, presumably because there are rarely true values outside of the predicted quantiles. They intersect for predictions of the first 2.5 km. Together with the Mean Squared Error (MSE) of the 0.5 quantile (median), this marks a prediction horizon for which a new prediction of the same segments in earlier than 2.5 km is assumed to be not significantly more precise. In this work, the control distance is therefore set to 2.5 km. It will be further analyzed in Section 3 when the predictive control is tested.
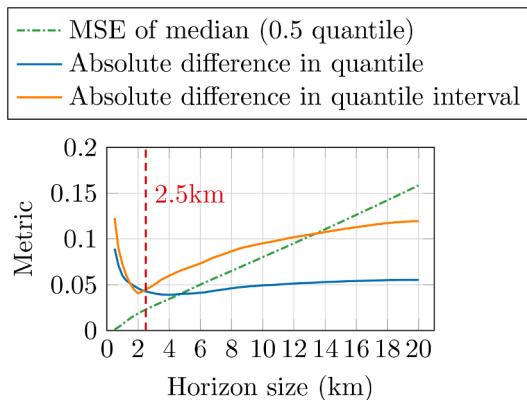

Fig. 2. Metrics of the QCNN on test data as given in [22], with better performance for lower values and calculated for different horizon sizes. The metrics include the Mean Squared Error (MSE) of the median prediction and the occurrence of true values within the predicted quantile and quantile interval. A dashed line marks the intersection of the two latter metrics.

2.2. QCNN Prediction

Battery temperature prediction is conducted by the best performing QCNN (model number 149) from [22] for five different battery cooling thresholds (25 °C, 30 °C, 35 °C, 40 °C, 45 °C). The QCNN consists of an input channel for history data and an input channel for foresight data. It uses 1D convolution layers and a custom loss function. It is trained on simulation, fleet and weather data[22]. provides more information about the model architecture, its hyperparameters, training and testing and the used data sets.

For each prediction, the requested cooling threshold needs to be set in addition to the preparation of input data described in subsection 2.1. Since training data did not cover changing thresholds, the threshold is set equally for both history and foresight horizon. The output of this step consists of seven quantile forecasts (0.01, 0.1, 0.25, 0.5, 0.75, 0.9, 0.99) in 250 m segments over the prediction horizon (20 km) for each of the five thresholds, which results in an output matrix with size (7, 80, 5). This output is used in the next step to choose the threshold with minimum costs.

2.3. Choice of battery cooling threshold

The predictive control chooses the battery cooling threshold with lowest total costs according to the predictions for the prediction horizon. The calculation steps are shown in Fig. 3. At first, cooling, ageing and derating costs are determined for each quantile prediction of each threshold. The calculation of the respective costs is described in the following paragraphs. The total costs per quantile and threshold $c_{q,t}$ are a weighted sum of the respective costs, with a cooling weight w_c, an ageing weight w_a and a derating weight w_d (1). The sum of the three weights is fixed to 1. The costs are averaged over all quantiles for each threshold, which leads to a single value of total costs per threshold c_t. The threshold with minimum costs is set as new threshold in the vehicle model, and only updated when the next control iteration starts after the control distance s_c is reached again. All cost functions are scaled into a range between 0 and 1, to achieve a similar order of magnitude for each cost term over the prediction horizon. Further balancing of the cost terms can be conducted by tuning their weights.

$$c_{q,t} = w_c \cdot c_c + w_a \cdot c_a + w_d \cdot c_d \tag{1}$$

2.3.1. Cooling costs

The activity of battery cooling in the prediction horizon is derived from the predicted battery temperature and the corresponding threshold with its fixed hysteresis of 2 °C. In the prediction example in Fig. 3, cooling costs would need to be calculated for each of the 250 m segments in the area between the two dashed lines. A tolerance value of 0.1 °C is set for the upper and lower bound of the hysteresis to cope with
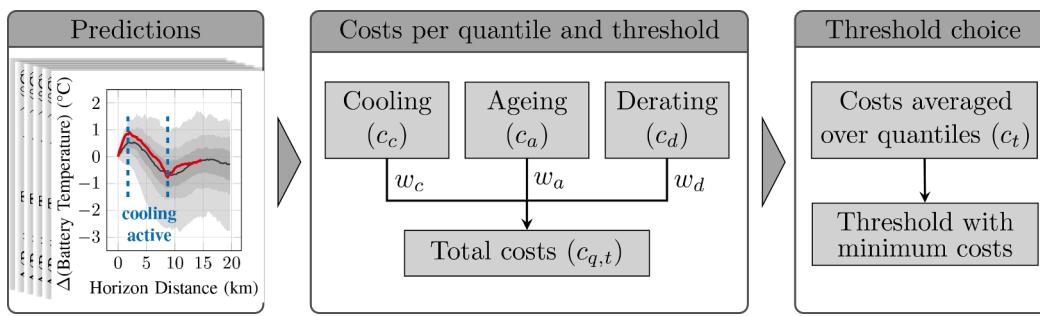
Fig. 3. Calculation steps leading from previously obtained predictions per threshold to the choice of a battery cooling threshold. The shown prediction example is taken from [22]. Costs are denoted by c and their cost weights by w.

inaccurate predictions. If end of drive (eod) occurs within the prediction horizon, predictions of segments exceeding it are neglected. For each quantile prediction, cooling costs are calculated as the number of all 250 m segments with active battery cooling. The result is divided by the total number of segments within the prediction horizon until end of drive, such that the cooling costs are scaled to a range between 0 and 1 before they are used in the weighted sum in (1).

2.3.2. Ageing costs

Ageing costs c_a are divided into costs for ageing during the drive $c_{a,d}$ and costs for calendric ageing after eod $c_{a,eod}$, when the vehicle is parked. The two parts are summed, including a weight $w_{a,eod}$ (2).

$$c_a = (1 - w_{a,eod}) \cdot c_{a,d} + w_{a,eod} \cdot c_{a,eod} \tag{2}$$

Ageing costs during the drive $c_{a,d}$ are calculated using a cost function $f_a(T_b)$ that depends on the predicted battery temperature T_b for each segment. In this work, the cost function $f_a(T_b)$ is based on [8] and is shown in Fig. 4. Compared with [8], it is scaled to a value of 1 at 45 °C, considering the highest available cooling threshold for QCNN predictions of 45 °C. Since ageing mechanisms depend on the battery cell and pack design, it needs to be adapted for later application in specific cars. The costs $c_{a,d}$ are calculated as the average of $f_a(T_b)$ of all segments within the prediction horizon, until end of drive if it occurs within the horizon.

Costs for calendric ageing after end of drive $c_{a,eod}$ depend on T_b, which can change during parking dependent on the ambient temperature T_{amb}. An approximation is necessary since the distance-based prediction model does not cover the time of a parked vehicle. Based on [30, p. 25–29], Eq. (3) describes the battery temperature change over time t of a parked vehicle (i.e. without battery discharge or charge). It depends on the difference between battery and ambient temperature, with the remaining quantities assumed to be constant. These quantities are the rate of heat transfer to the vehicle surroundings $\dot{Q}_s$, battery mass m_b, specific heat capacity of the battery $c_{p,b}$, a combined heat transfer coefficient h_s and surface A_s.
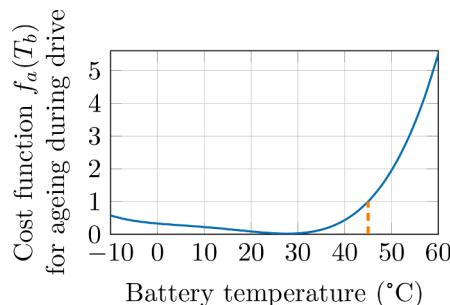
$$\frac{\partial T_b(t)}{\partial t} = \frac{\dot{Q}_s}{m_b \cdot c_{p,b}} = \frac{h_s A_s (T_b - T_{amb})}{m_b \cdot c_{p,b}} \tag{3}$$

The equation is further simplified to (4) using τ, which replaces the parameters h_s, A_s, m_b and $c_{p,b}$ as a constant. The constant is empirically determined based on vehicle fleet data which contain T_b and T_{amb}, using the first value of a drive and the last value of the previous drive. Data is collected from the same vehicle fleet than in [22], but for an extended time range of March 2021 until April 2022. Only data with parking times between 10 min and 6 h are considered in order to exclude unwanted side effects (e.g. due to weather changes during longer parking times). Additional filtering addresses implausible data and data with battery temperatures at end of drive lower than 20 °C, since this work focuses on cooling behavior at higher temperatures. After all filtering steps, the data set consists of 226 drives from 11 vehicles. Curve fitting provides a value of $\tau = -0.1163$, with the fitted curve shown in Fig. 5.

$$f_{cooldown}(T_b, T_{amb}) = \frac{\partial T_b(t)}{\partial t} = \tau \cdot (T_b - T_{amb}) \tag{4}$$

The cost function for end of drive ageing is given by (5). Costs are calculated only if the end of drive is within the prediction horizon, using the predicted battery temperature of the segment at the end of drive $T_{b,eod}$ and the given ambient temperature $T_{amb,eod}$. The exponential function provides positive, decreasing cost values with an increase in temperature difference between $T_{b,eod}$ and $T_{amb,eod}$. Note that this exponential function does not describe Newton's law of cooling [31].

$$c_{a,eod} = f_a(T_{b,eod}) \cdot \exp(f_{cooldown}(T_{b,eod}, T_{amb,eod})) \tag{5}$$

Fig. 4. Cost function for temperature dependent battery ageing based on [8], after scaling to 1 at 45 °C as marked by the dashed line.
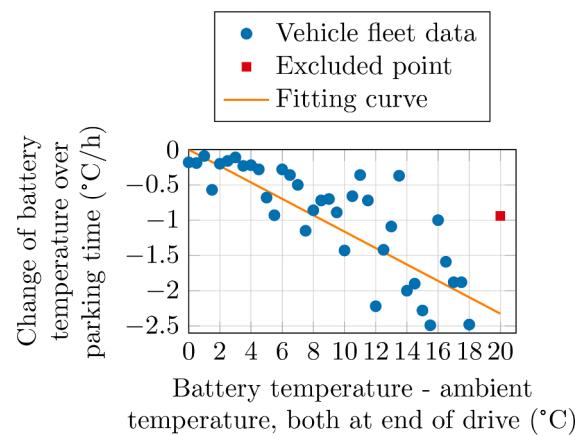

Fig. 5. Curve fitting of the battery temperature change of a parked vehicle using vehicle fleet data. Each point represents the average value of all observed rates (y-axis) within buckets of 0.5 °C for the corresponding difference in temperatures at end of drive (x-axis).

2.3.3. Derating costs

Derating costs describe the T_b-dependent limitation of maximum available power by the battery management system. In this work, they are defined by (6), with a scaling to 1 at 50 °C battery temperature, since the battery temperature is assumed to not exceed 50 °C in most cases. The costs are calculated as average of all predicted segments k in the prediction horizon until eod. Segments after eod are excluded from the calculation. A prediction of the requested power is not included, such that the costs are evaluated even when less than the maximum available power might be requested by the driver. Derating at low battery temperatures is also neglected in this work due to its focus on battery cooling rather than heating.

$$c_d = \frac{1}{k} \sum_{i=1}^{k} \left(\frac{T_{b,i} - 40°C}{10°C} \text{ if } T_{b,i} \geq 40°C, \ 0 \text{ otherwise} \right) \quad (6)$$

2.4. Drive profiles for analysis

The analysis of the developed predictive battery thermal management covers its adaptability, tunability and robustness, as shown in Fig. 6. The simulated drive profiles consist of the US06 drive cycle (noted by D) [32], the Urban (U), Rural (R) and Highway (H) parts of the Artemis drive cycle [33] and the aggressive drive profile from Tzirakis et al. (T) [34]. The Design Of Experiments (DOE) used for tunability and robustness analysis is given by Table 1. The ambient temperature T_{amb} and initial battery temperature $T_{b,init}$ are varied to cover different cases of battery cooling with respect to a fixed threshold of 35 °C (e.g. cooling activation during drive or from the beginning). T_{amb} is kept constant during each simulation. In total, the DOE consists of 18 scenarios.

Two types of foresight input noise are used for robustness analysis. An overview is given by Table 2. Gaussian noise is considered to represent a more dynamic forecast (MD) than the actual profile. The noise is added after smoothing it with a moving average with a centered window of size 5. A less dynamic forecast (LD) than actual is considered using a centered moving average for the speed and the same Gaussian noise for elevation as for MD.

3. Results

An application of the predictive BTMS is presented in this chapter. It covers an exemplary analysis with respect to adaptability, tunability and robustness. The influence of the control distance s_c is examined, as well as the energy saving potential. A brief overview on computation times of the predictive control is included.

3.1. Adaptability

The developed predictive BTMS is designed to adapt battery cooling thresholds to the battery temperature prediction and its foresight input data. Fig. 7 shows an example of two scenarios with the last section (after 55.3 km) differing in elevation and speed. For this specific

Table 1
Design Of Experiments (DOE) with 18 scenarios. The elevation for each section is denoted by '_' for zero slope, '↑' for positive slope θ and '↓' for negative slope $-\theta$. A digit in front of a section (H, D, U, R or T) indicates the number of repetitions. Each profile is simulated with varying ambient temperature T_{amb} and initial battery temperature $T_{b,init}$. This leads to 18 scenarios, as accordingly numbered in the first column.

Scenario	Profile	Elevation	T_{amb} (°C)	$T_{b,init}$ (°C)	$|\theta| \ \forall (\uparrow, \downarrow)$ (m/km)
1/2/3/4	H D D D	_ ↑ ↓ ↑	30/30/25/30	33.5/38/33.5/30	20
5/6/7/8	H D D U U	_ ↑ ↓ _ _	30/30/25/30	33.5/38/33.5/30	20
9/10/11/12	H R U U	_ _ _ _	30/30/25/30	33.5/38/33.5/30	20
13/14/15	12T	3↓ 3↑ 3↓ 3↑	30/20/30	30/25/38	50
16/17/18	9T U U	3↓ 3↑ 3↓ _ _	30/20/30	30/25/38	50

Table 2
Noise types added to foresight input data. Gaussian noise is defined by mean value μ and standard deviation σ, centered moving average by window size.

Noise type	Speed	Elevation
More Dynamic (MD)	Gaussian noise ($\mu = 0$ km/h, $\sigma = 20$ km/h)	Gaussian noise ($\mu = 0$ m, $\sigma = 4$ m)
Less Dynamic (LD)	Centered moving average (window size 9)	Gaussian noise ($\mu = 0$ m, $\sigma = 4$ m)

exemplary analysis, the weights are set to $w_c = 0.08, w_a = 0.72, w_{a,eod} = 0.2$ and $w_d = 0.2$ such that the influence of the profile can be seen clearly. The total costs at each prediction and control step are calculated for all five cooling thresholds. Fig. 7 (c) and (d) show the total costs based on predictions with corresponding cooling thresholds. T_b and the battery cooling thresholds that are chosen by the predictive BTMS are included in Fig. 7 (e) and (f) for both scenarios.

In the first scenario (Fig. 7 (a),(c),(e)), the cooling threshold is once raised from 35 °C to 40 °C after 17.5 km when the predicted costs for a threshold of 35 °C are higher than for 40 °C. The higher cooling threshold prevents battery cooling in this scenario and is not changed by the predictive BTMS until end of drive. In comparison with a fixed cooling threshold of 35 °C, the total energy consumption is reduced by 0.62% for this scenario and the given set of weights.

In the second scenario (Fig. 7 (b),(d),(f)), the predicted costs start to differ after 35 km compared to the first scenario due to different predictions for the last section. Cooling is activated after 47.5 km, before the last section is reached. In Fig. 7 (d), the magnifier box shows the corresponding segments at which the costs are lower for 35 °C and 25 °C than for 40 °C (first two vertical lines) and battery cooling is active. This is due to higher predicted costs for a threshold of 40 °C compared to the first scenario (shown as dotted line), since the last section leads to a higher (predicted) heat generation of the battery. The battery cooling
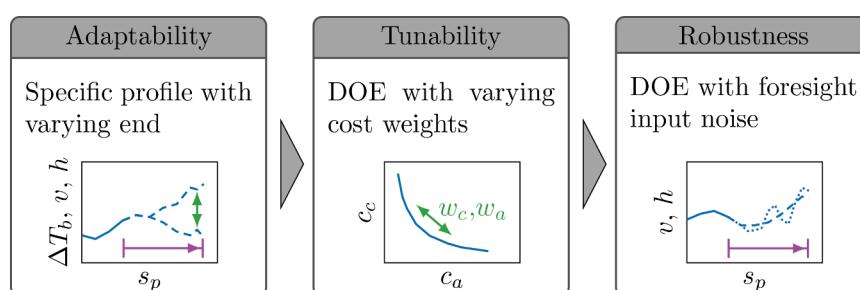
Fig. 6. The analysis of the developed predictive control includes the effect of variation of input foresight data (speed v, height h) and cost weights (ageing w_a, cooling w_c) on the predicted change in battery temperature T_b over the prediction horizon s_p and the resulting costs (ageing c_a, cooling c_c). The DOE is shown in Table 1.
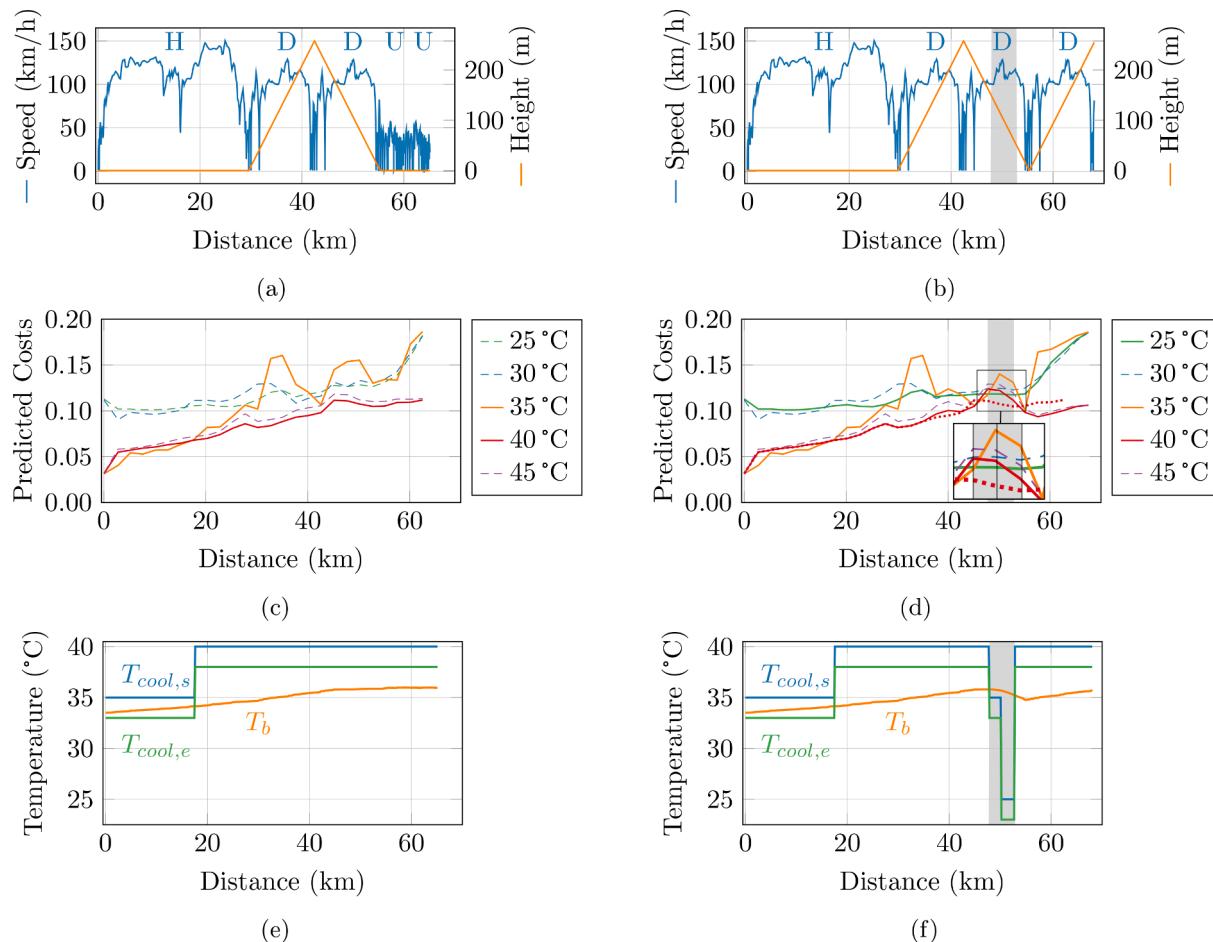
Fig. 7. Drive profiles HDDUU and HDDD are shown in (a) and (b). (c) and (d) depict the calculated costs based on the prediction for each cooling threshold, with the less relevant thresholds as dashed line. In the magnifier in (d), vertical lines indicate prediction steps. The costs for a threshold of 40 °C with profile HDDUU are included in (d) as a dotted line. Battery temperature T_b and cooling threshold with start $T_{cool,s}$ and end $T_{cool,e}$ are shown in (e) for HDDUU and in (f) for HDDD. A gray shaded area marks active battery cooling in (b),(d),(f).

threshold is not kept low for the prediction horizon of 20 km, but it is updated to 40 °C once the battery temperature is lower due to active cooling (third vertical line in magnifier box). The lower temperature results in lower, predicted costs for the last section even without cooling. Compared to a fixed threshold of 35 °C, cooling time is reduced by 65%

and total energy consumption by 1.02%. The analysis shows the ability of the predictive BTMS to proactively adapt to different drive profiles ahead.
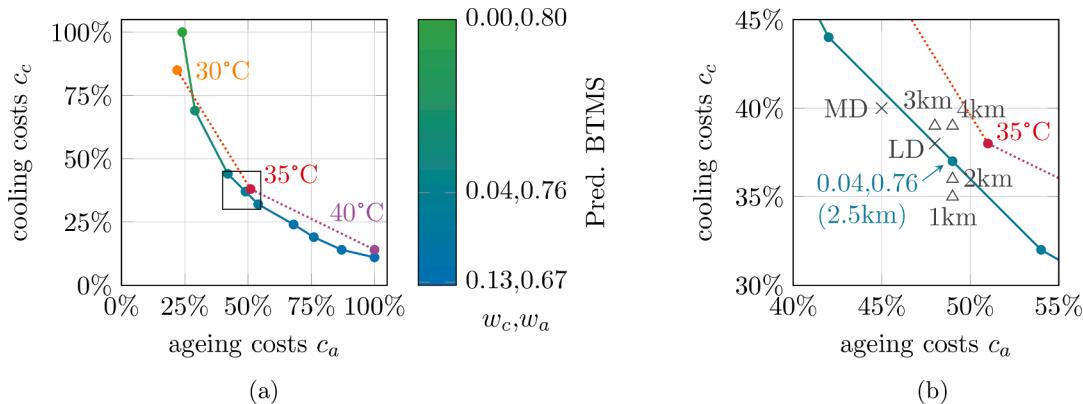

Fig. 8. Average cooling and ageing costs are shown in (a) for DOE simulations with varied cooling (w_c) and ageing (w_a) weights as indicated by the colorbar. A dotted line connects the costs for fixed thresholds 30 °C, 35 °C and 40 °C. The section of the black rectangle is displayed in (b). Crosses show the results for the weight set (0.04,0.76) with input noise (more dynamic, MD, and less dynamic, LD). Triangles show results with the same weights but a varied control interval (from 1 km to 4 km), while 2.5 km was used for all other simulations. (For interpretation of the references to colour in this figure legend, the reader is referred to the web version of this article.)

3.2. Tunability

All 18 DOE scenarios (see Table 1) are simulated for nine different sets of cooling and ageing weights (w_c, w_a), varying from (0.0,0.8) to (0.13,0.67). The derating weight w_d is kept constant at 0.2 and $w_{a,eod}$ is fixed to 0.2. The resulting cooling and ageing costs are averaged over all 18 scenarios for each weight setting and scaled by the maximum value, as shown in Fig. 8 (a). They form a Pareto curve, with the weight set (0.04,0.76) being closest to the theoretical optimum of zero costs (0%,0%). It is also closest to a slope of -1, at which a decrease in one cost type results in an equal increase of the other cost type. The resulting costs for the same DOE with fixed thresholds 30 °C, 35 °C and 40 °C is included. In comparison, the Pareto curve of the predictive BTMS is closer to the theoretical optimum except for the weight set (0.0,0.8). The analysis shows the tunability of the predictive control as well as its potential to reduce cooling and ageing costs.

3.3. Robustness and influence of control distance

The influence of foresight input noise on the weight set (0.04,0.76) is depicted by gray crosses in Fig. 8 (b). The result with a more dynamic forecast (MD) than actual results in higher cooling but lower ageing costs, since the prediction model overestimates the rise in battery temperature which leads to more cooling. A less dynamic forecast (LD) results in a smaller difference, again with higher cooling and lower ageing costs. In both cases, the resulting costs with input noise are in a similar range than without, and closer to the optimum than for the fixed threshold strategy. According to this analysis, the model shows good robustness to uncertainty of the foresight input data.

Predictions and threshold adaptions are conducted in an interval of 2.5 km. The weight set (0.04,0.76) is simulated additionally with intervals of 1 km, 2 km, 3 km and 4 km to analyse the effect of the control distance s_c. The results are shown as triangles in Fig. 8 (b). In all cases the resulting costs are closer to the theoretical optimum of zero costs than for the fixed threshold of 35 °C.

3.4. Energy consumption reduction

A comparison of cooling and ageing costs between the results with a fixed threshold of 35 °C and the results with predictive control is shown in Fig. 9. The reduction of cooling costs represents the reduction of battery cooling energy consumption. Additionally, the effect of reduced battery cooling on total energy consumption is calculated. Using predictive control with weights (0.04,0.76), cooling costs are reduced by 4% and ageing costs are lowered by 5%. The total energy consumption is reduced by 0.06%. Additional simulations of the DOE with weights (0.0485,0.7515) lead to the same ageing costs than for a fixed threshold of 35 °C, such that the result is located at a x-value of zero in Fig. 9. As a result, a reduction of cooling costs by 9% and of energy consumption by

Fig. 9. Comparison of cooling costs and ageing costs with respect to the results with a fixed threshold of 35 °C. The weight set (0.0485,0.7515) shows a potential reduction of cooling costs by -9% with same ageing costs.

0.11% is possible with the same ageing costs. The scenario with the highest energy saving potential with this weight set is the 12T profile with T_{amb} and $T_{b,init}$ equal to 30 °C. In this scenario cooling costs are reduced by 34% and total energy consumption by 0.57%.

Further improvements in energy consumption will lead to higher ageing, thus reduced lifetime, than for the fixed threshold of 35 °C. Accordingly, the weights of the predictive BTMS can also be tuned to increase battery lifetime taking higher energy consumption into account. The developed control offers these possibilities, which can be used dependent on a holistic consideration of energy consumption and lifetime for the according BEV.

3.5. Computation time

An analysis of the computation time during all simulations considers a separate time measurement of each simulation step, prediction step and step of threshold choice. The used hardware consists of an Intel i7 (3.0 GHz) processor and 16 GB RAM. However, the predictive control does not need the full computational capacity of this hardware. The simulations are conducted with Python 3.7.5, using TensorFlow/Keras package version 2.5.0 for the QCNN.

The following times are measured for simulations of all DOE profiles with the weight set (0.0485,0.7515). The time measurement of the prediction step includes the time needed for normalization and denormalization of inputs and outputs and covers the predictions for all five thresholds. The prediction step takes on average 1.11 s, the threshold choice step on average 0.03 s. The sum of maximum prediction time and maximum threshold choice time is 3.63 s, which equals a speed of 248 km/h that is needed to drive a distance of 250 m during that time. Thus, for speeds lower than that value, the predictive control is fast enough to set a new threshold before the next 250 m segment is reached. Setting the new threshold for the following 250 m segment is important for the control performance since the QCNN predictions assume the new threshold for all segments, including the one that immediately follows.

4. Discussion

The usage of a QCNN for battery temperature prediction enables a proactive adaption of the battery cooling threshold. The proposed predictive BTMS shows better performance than a fixed threshold control, considering ageing and cooling costs. While the analysis shows the potential to improve the BTMS performance for both cooling and ageing costs, there are several aspects of the model and its evaluation that can be improved.

In this work, prediction and choice of cooling thresholds are conducted only in a fixed interval of 2.5 km. This control distance can be further optimized, for example adapted to the boundary conditions (e.g. longer during highway drive, shorter during urban drive). Due to the distance-based control interval, the proposed predictive BTMS does not adapt the cooling threshold during times where the vehicle is standing. In comparison with a time-based interval, it is acceptable due to the following reasons: Firstly, battery cooling is still activated or deactivated according to the last chosen threshold, such that the battery will not reach too high temperatures. Secondly, the battery temperature is expected to not change significantly during standing (except for active cooling) since the main input parameters do not (significantly) change at that time. This includes velocity, height profile and ambient temperature for shorter time periods.

The number of predefined thresholds is limited to five and only a fixed value can be chosen for the prediction horizon of 20 km in every control interval. On the one hand, this limits the freedom of adapting the battery cooling threshold and minimizing costs. On the other hand, it leads to low computation times since only five cases need to be evaluated. The hysteresis and control distance also prevent high stress for BTMS components which could occur with more frequent changes. In
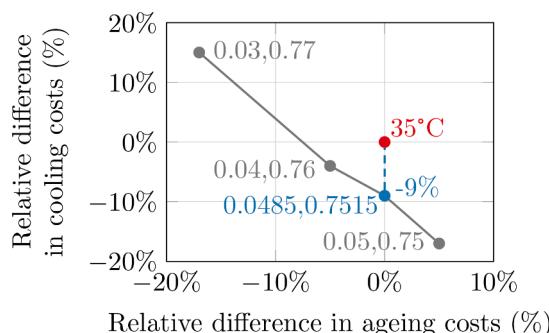
future works, the prediction model can be optimized online to adapt to individual driver behavior and regional climate conditions.

The calculation of costs requires an accurate battery temperature prediction. An optimization of the QCNN, as discussed in [22], is expected to further improve the BTMS performance. For example, the calculation of cooling costs highly depends on the prediction accuracy due to the indirect identification of active cooling using the predicted temperature and the corresponding threshold. The dependence of cooling power on other quantities can be added for a more holistic estimation of cooling costs, for instance using ambient temperature, cabin cooling, coolant temperature or efficiency of BTMS components. Ageing costs can be extended by their dependency on the SOC and an estimation of parking time after eod. Derating costs can be combined with a prediction of the actual power demand as well as the usable fast charging power on the battery temperature at eod in case of an upcoming fast-charging event. Similar to an online optimization of the prediction model, the cost weights can be adapted to individual drivers, regions and to driving modes (e.g. a sports mode versus an eco mode). Using Reinforcement Learning methods, the predictive control can be developed and optimized continuously based on resulting costs as feedback.

Evaluation of the predictive control is based on a fixed DOE with limited variance in profiles and boundary conditions. The DOE needs to be extended by more variance, for instance by profiles from fleet data, since the profiles and boundary conditions have a big impact on the energy reduction potential. The exemplary analysis of varying input profiles shows plausible adaptability of the cooling threshold, but a more holistic sensitivity analysis may provide further insights about the performance in later applications. The tunability analysis can be used to identify the preferred set of weights, but needs to be extended by all remaining weights and design parameters (in this work $w_{a,eod}$, w_d and s_c). Furthermore, only the average of each cost term is considered in the comparison of weight sets. The developed predictive control proved to be robust to foresight input noise, while further variance in noise can give a deeper understanding about its robustness and limitations. Strong deviations from the input foresight data could however lead to worse performance, for example when the driver spontaneously changes the route.

Given a larger DOE, the impact on energy consumption and State Of Health (SOH) should be further analyzed to provide more tangible key metrics than predefined cost terms. Besides the consideration of a fixed threshold control, a comparison with other predictive control methods might give more insights about potential and limitations of the developed method. The evaluation of computation times needs to be repeated with the according hardware of later application. Alternatively, the prediction could be conducted in a cloud system, if data transfer between backend and vehicle is fast enough for the used sampling and control distance. In future works, the developed predictive BTMS needs to be tested in a real car to fine-tune its weights and validate the results.

The proposed predictive control showed a reduction in both cooling and ageing costs. Considering the efforts for training the QCNN and for implementation of the predictive control, further improvements in energy consumption or ageing should be targeted. For instance, a more accurate prediction model and more choices of control variables may be advantageous. The energy saving potential also depends on the given BTMS components, vehicle specifications and driving profile. For example, the saved cooling energy has a lower impact on total energy consumption in case of a dynamic profile with high energy consumption caused by acceleration. The developed control might show more potential for energy consumption reduction in other applications, for example to adapt heating thresholds or for BTMS of hybrid electric vehicles or thermal management of the electric machine. It can be also used for predictive control applications outside the automotive sector.

5. Conclusion

This work presented a predictive control of a Battery Thermal Management System (BTMS) using a Quantile Convolutional Neural Network (QCNN) for battery temperature prediction and cost functions for cooling, ageing and derating. The main contributions and results consist of the following:

- Battery temperature predictions of a QCNN enabled the calculation of different types of costs for the prediction horizon in order to choose the most suitable cooling threshold.
- The cost functions were partly derived by empirical or physical dependencies and the quantile predictions allowed a direct consideration of the prediction uncertainty.
- Simulations with different routes ahead led to different predicted costs. Consequently, the predictive BTMS proactively adapted the cooling threshold accordingly, proving its adaptability.
- A Pareto curve indicated the effect of varied cooling and ageing weights on the contradicting optimization goals, representing the tunability of the predictive BTMS.
- Induced noise on the foresight input data resulted in low variation of ageing and cooling costs which confirmed the robustness of the proposed approach.
- The predictive BTMS performed better than a fixed threshold control considering cooling and ageing costs. On average over 18 simulated scenarios, cooling costs could be reduced by 9% with unchanged ageing costs.

Further extensions and optimization of the predictive control could target the cooling threshold variation, the accuracy of the QCNN, the calculation of cost functions and performance evaluation. Such an optimized control should be compared with other predictive control methods and applied in other domains to further understand its potentials.

Declaration of Competing Interest

The authors declare that they have no known competing financial interests or personal relationships that could have appeared to influence the work reported in this paper.

Data Availability

The data that has been used is confidential.

Acknowledgment

References

[1] G. Conway, A. Joshi, F. Leach, A. García, P.K. Senecal, A review of current and future powertrain technologies and trends in 2020, Transp. Eng. 5 (2021) 100080, https://doi.org/10.1016/j.treng.2021.100080.

[2] Y. Zheng, X. He, H. Wang, M. Wang, S. Zhang, D. Ma, B. Wang, Y. Wu, Well-to-wheels greenhouse gas and air pollutant emissions from battery electric vehicles in china, Mitig. Adapt. Strateg. Glob. Chang. 25 (3) (2020) 355–370, https://doi.org/10.1007/s11027-019-09890-5.

[3] A. Enthaler, T. Weustenfeld, F. Gauterin, J. Koehler, Thermal management consumption and its effect on remaining range estimation of electric vehicles. Proceedings of the International Conference on Connected Vehicles and Expo (ICCVE), IEEE, Vienna, Austria, 2014, pp. 170–177.

[4] S. Park, C. Ahn, Stochastic model predictive controller for battery thermal management of electric vehicles. Proceedings of the IEEE Vehicle Power and Propulsion Conference (VPPC), IEEE, Hanoi, Vietnam, 2019, pp. 1–5.

[5] Y. Xie, C. Wang, X. Hu, X. Lin, Y. Zhang, W. Li, An MPC-based control strategy for electric vehicle battery cooling considering energy saving and battery lifespan,

IEEE Trans. Veh. Technol. 69 (12) (2020) 14657–14673, https://doi.org/10.1109/TVT.2020.3032989.

[6] S. Park, C. Ahn, Model predictive control with stochastically approximated cost-to-go for battery cooling system of electric vehicles, IEEE Trans. Veh. Technol. 70 (5) (2021) 4312–4323, https://doi.org/10.1109/TVT.2021.3073126.

[7] T. Fischer, T. Kraus, C. Kirches, F. Gauterin, Nonlinear model predictive control of a thermal management system for electrified vehicles using FMI. Proceedings of the 12th International Modelica Conference, in: Linköping Electronic Conference Proceedings, Linköping University Electronic Press, Prague, Czech Republic, 2017, pp. 255–264, https://doi.org/10.3384/ecp17132255.

[8] J. Lopez-Sanz, C. Ocampo-Martinez, J. Alvarez-Florez, M. Moreno-Eguilaz, R. Ruiz-Mansilla, J. Kalmus, M. Graeber, G. Lux, Thermal management in plug-in hybrid electric vehicles: a real-time nonlinear model predictive control implementation, IEEE Trans. Veh. Technol. 66 (9) (2017) 7751–7760, https://doi.org/10.1109/TVT.2017.2678921.

[9] C. Zhu, F. Lu, H. Zhang, C.C. Mi, Robust predictive battery thermal management strategy for connected and automated hybrid electric vehicles based on thermoelectric parameter uncertainty, IEEE J. Emerg. Sel. Top. Power Electron. 6 (4) (2018) 1796–1805, https://doi.org/10.1109/JESTPE.2018.2852218.

[10] D. van der Meer, G.C. Wang, J. Munkhammar, An alternative optimal strategy for stochastic model predictive control of a residential battery energy management system with solar photovoltaic, Appl. Energy 283 (2021) 116289, https://doi.org/10.1016/j.apenergy.2020.116289.

[11] S. Zhao, A.M. Reza, S. Jing, C.C. Mi, A two-layer real-time optimization control strategy for integrated battery thermal management and HVAC system in connected and automated HEVs, IEEE Trans. Veh. Technol. 70 (7) (2021) 6567–6576, https://doi.org/10.1109/TVT.2021.3085938.

[12] S. Zhao, C.C. Mi, A two-stage real-time optimized ev battery cooling control based on hierarchical and iterative dynamic programming and MPC: early access, IEEE Trans. Intell. Transp. Syst. (2021) 1–11, https://doi.org/10.1109/TITS.2021.3106253.

[13] Y. Liu, J. Zhang, Self-adapting intelligent battery thermal management system via artificial neural network based model predictive control. Volume 2A: 45th Design Automation Conference, American Society of Mechanical Engineers, Anaheim, California, USA, 2019, https://doi.org/10.1115/DETC2019-98205.

[14] J. Park, Y. Kim, Supervised-learning-based optimal thermal management in an electric vehicle, IEEE Access 8 (2020) 1290–1302, https://doi.org/10.1109/ACCESS.2019.2961791.

[15] Y. Jiang, Y. Yu, J. Huang, W. Cai, J. Marco, Li-ion battery temperature estimation based on recurrent neural networks, Sci. China Technol. Sci. 64 (2021), https://doi.org/10.1007/s11431-020-1736-5.

[16] J. Park, Z. Chen, L. Kiliaris, M.L. Kuang, M.A. Masrur, A.M. Phillips, Y.L. Murphey, Intelligent vehicle power control based on machine learning of optimal control parameters and prediction of road type and traffic congestion, IEEE Trans. Veh. Technol. 58 (9) (2009) 4741–4756, https://doi.org/10.1109/TVT.2009.2027710.

[17] A. Kempf, E. Weber, S. Müller, A multi model neural network approach for longitudinal model predictive control of a passenger vehicle. Proceedings of the 2020 IEEE 23rd International Conference on Intelligent Transportation Systems (ITSC), IEEE, Rhodes, Greece, 2020, pp. 1–6.

[18] F. Deufel, M. Gießler, F. Gauterin, A generic prediction approach for optimal control of electrified vehicles using artificial intelligence, Vehicles 4 (1) (2022) 182–198, https://doi.org/10.3390/vehicles4010012.

[19] Y. Jeong, S. Kim, K. Yi, Surround vehicle motion prediction using LSTM-RNN for motion planning of autonomous vehicles at multi-lane turn intersections, IEEE Open J. Intell. Transp. Syst. 1 (2020) 2–14, https://doi.org/10.1109/OJITS.2020.2965969.

[20] J.W. Moon, J.-J. Kim, Ann-based thermal control models for residential buildings, Build. Environ. 45 (7) (2010) 1612–1625, https://doi.org/10.1016/j.buildenv.2010.01.009.

[21] A. Vasičkaninová, M. Bakošová, A. Mészáros, J.J. Klemeš, Neural network predictive control of a heat exchanger, Appl. Therm. Eng. 31 (13) (2011) 2094–2100, https://doi.org/10.1016/j.applthermaleng.2011.01.026.

[22] A.M. Billert, M. Frey, F. Gauterin, A method of developing quantile convolutional neural networks for electric vehicle battery temperature prediction trained on cross-domain data, IEEE Open J. Intell. Transp. Syst. 3 (2022) 411–425, https://doi.org/10.1109/OJITS.2022.3177007.

[23] F. Leng, C.M. Tan, M. Pecht, Effect of temperature on the aging rate of li ion battery operating above room temperature, Sci. Rep. 5 (1) (2015) 12967, https://doi.org/10.1038/srep12967.

[24] L. Spitthoff, P.R. Shearing, O.S. Burheim, Temperature, ageing and thermal management of lithium-ion batteries, Energies 14 (5) (2021) 1248, https://doi.org/10.3390/en14051248.

[25] J.V. Barreras, T. Raj, D.A. Howey, Derating strategies for lithium-ion batteries in electric vehicles. Proceedings of the IECON 2018 - 44th Annual Conference of the IEEE Industrial Electronics Society, IEEE, Washington, DC, USA, 2018, pp. 4956–4961.

[26] Y. Sun, S. Saxena, M. Pecht, Derating guidelines for lithium-ion batteries, Energies 11 (12) (2018) 3295, https://doi.org/10.3390/en11123295.

[27] M. Schwenzer, M. Ay, T. Bergs, D. Abel, Review on model predictive control: an engineering perspective, Int. J. Adv. Manuf. Technol. 117 (5) (2021) 1327–1349, https://doi.org/10.1007/s00170-021-07682-3.

[28] M.V. Prati, M.A. Costagliola, R. Giuzio, C. Corsetti, C. Beatrice, Emissions and energy consumption of a plug-in hybrid passenger car in real driving emission (rde) test, Transp. Eng. 4 (2021) 100069, https://doi.org/10.1016/j.treng.2021.100069.

[29] X. Kuang, K. Li, Y. Xie, C. Wu, P. Wang, X. Wang, C. Fu, Research on control strategy for a battery thermal management system for electric vehicles based on secondary loop cooling, IEEE Access 8 (2020) 73475–73493, https://doi.org/10.1109/ACCESS.2020.2986814.

[30] Y.A. Cengel, Heat transfer: A Practical Approach, 2nd, McGraw-Hill, New York, NY, USA, 2002.

[31] S. Lavety, A.P. Bhale, K.R. Kumar, M.A. Chaudhari, Electro-thermal model of traction battery for regulated pulse charging. Proceedings of the IECON 2017 - 43rd Annual Conference of the IEEE Industrial Electronics Society, IEEE, Beijing, China, 2017, pp. 2270–2274.

[32] United States Environmental Protection Agency, Dynamometer drive schedules, 2021, dynamometer-drive-schedules. Accessed June 02, 2022, https://www.epa.gov/vehicle-and-fuel-emissions-testing/dynamometer-drive-schedules.

[33] M. André, The artemis european driving cycles for measuring car pollutant emissions, Sci. Total Environ. 334–335 (2004) 73–84, https://doi.org/10.1016/j.scitotenv.2004.04.070.

[34] E. Tzirakis, F. Zannikos, S. Stournas, Impact of driving style on fuel consumption and exhaust emissions: defensive and aggressive driving style. Proceedings of the 10th International Conference on Environmental Science and Technology, Kos, Greece, 2007, pp. 1497–1504.